Available online at www.sciencedirect.com
SCIENCE DIRECT®
Journal of Nuclear Materials 337–339 (2005) 381–385
journal of nuclear materials
www.elsevier.com/locate/jnucmat

Multi-machine comparisons of H-mode separatrix densities and edge profile behaviour in the ITPA SOL and Divertor Physics Topical Group

A. Kallenbach [a,*], N. Asakura [b], A. Kirk [c], A. Korotkov [c], M.A. Mahdavi [d], D. Mossessian [e], G.D. Porter [f]

[a] *Max-Planck-Institut für Plasmaphysik, IPP-EURATOM Association, Boltzmannstr. 2, D-85748 Garching, Germany*
[b] *Japan Atomic Energy Research Institute, Naka-machi, Naka-gun, Ibaraki 311-0193, Japan*
[c] *EURATOM/UKAEA Fusion Association, Culham Science Centre, Abingdon, Oxon OX14 3DB, UK*
[d] *General Atomics, P.O. Box 85608, San Diego, CA 92186-5608, USA*
[e] *MIT Plasma Science and Fusion Center, 175 Albany st., Cambridge, MA 02139, USA*
[f] *Lawrence Livermore National Laboratory, P.O. Box 808, Livermore, CA 94550, USA*

Abstract

Edge profile data for H-mode discharges in 6 tokamaks have been analysed with the main focus on the edge density profile as well as electron temperature and density gradient lengths and steep gradient zone widths. A uniform procedure of data treatment and assignment of the separatrix position via power balance allowed to put the multi-machine data on an even base. The machine size appears to be the leading parameter for the width of the steep edge transport barrier gradient zone, as well as for the temperature decay length at the separatrix. Effects associated with neutral penetration physics are visible in the edge density profile.

PACS: 52.55.Fa; 52.25.Fi; 52.65.−y
Keywords: Edge transport; Hydrogen recycling; SOL plasma

1. Introduction

The separatrix density is a key parameter for divertor particle and energy exhaust since divertor radiated power and neutral pressure increase non-linearly with the separatrix density up to the detachment point. A new multi-machine database for the separatrix density and surrounding electron density and temperature profiles for H-mode conditions has been set up in the ITPA Topical Group on Scrape-Off Layer and Divertor Physics. The main objectives are to understand the physics which determines the density profile around the separatrix and its impact on pedestal properties as well as the temperature decay length at the separatrix.

2. Multi-machine data base

The profile data consist of electron density and temperature measurements in the edge/pedestal region

* Corresponding author. Tel.: +49 89 3299 1721; fax: +49 89 3299 1812.
E-mail address: arne.kallenbach@ipp.mpg.de (A. Kallenbach).

0022-3115/$ - see front matter © 2004 Elsevier B.V. All rights reserved.
doi:10.1016/j.jnucmat.2004.10.099

measured by Thomson scattering in Alcator C-Mod [1], ASDEX Upgrade (AUG) [2], DIII-D [3], MAST [4], JET [5] and JT-60U [6]. The JET edge LIDAR data have been combined with Lithium beam measurements and other diagnostics and regularized by EDGE2D modelling in order to improve the spatial coverage and resolution [7]. The JT-60U Thomson data are supplemented by Langmuir probe measurements in the main chamber scrape-off layer (SOL) [8]. All data are taken time-averaged for ELMy H-mode conditions, mapped to the outer midplane and regularized by fitting a modified tanh function [2]. The power law analyses are based on the profile characteristics as described by the mtanh fit and additional scalar data (plasma current I_p, stored energy W_{MHD}, etc.). The MAST ELMs cannot be clearly assigned to type-I, but the profile data are particularly valuable for the aspect ratio dependence (MAST lies around 1.5, while the other machines have $R/a = 2.9$–3.6).

Since the equilibrium reconstruction is generally not accurate enough in the presence of steep H-mode edge gradients, the separatrix position is assigned by the power flow. We use the upstream temperature T_u as defined by

$$T_u = (T_{div}^{7/2} + 7/2(P_{heat} - P_{rad}) \cdot L_{con}/(A_{q\|} \cdot \kappa_0))^{2/7} \qquad (1)$$

as best available estimate for the experimental separatrix temperature $T_{e,sep}$. The divertor temperature T_{div} is assumed to be 0 for simplicity. $L_{con} = \pi R_0 q_{95}$ is the connection length (for the spherical tokamak MAST, the value from equilibrium reconstruction is used). $A_{q\|} = 4\pi R_0 \lambda_{q\perp} B_p/B$ is the surface area for the parallel power flux, with the radial power decay length $\lambda_{q\perp} = 2/7\lambda_{T_e}$. Dominant electron thermal conductivity is assumed here, which results in T_u becoming more uncertain for conditions with low ion collisionality [9]. In the case of MAST, the Thomson scattering data do not allow to reliably determine the T_e decay length at the separatrix, therefore, a typical value $\lambda_{q\perp} = 8$ mm obtained from probe measurements is used to calculate T_u.

For the database analysis, the experimental T_e profiles are shifted in radial direction to obtain $T_{e,sep} = T_u$, the electron density profiles are shifted accordingly since Thomson scattering data for n_e and T_e are measured at identical locations.

Fig. 1 shows the separatrix and pedestal densities in the database. $n_{e,sep}$ varies by 2 orders of magnitude from JT-60U to C-Mod, the variation of the pedestal density is slightly smaller. As can be seen in Fig. 1(b), the ratio $n_{e,ped}/n_{e,sep}$, which constitutes the most important fraction of the core density gain within the edge transport barrier (ETB), is reduced with increasing Greenwald fraction of the separatrix density. The lower limit of the H-mode density is determined by machine conditioning in terms of hydrogen wall release and pumping speed. The ITER reference point lies already above the bulk of present day machine data. However, a physics model for the density buildup is required to predict the ITER value. The normalisation by the Greenwald density has been proven to be empirically quite successful for many tokamaks, but the underlying physics has not been fully resolved.

2.1. Neutral penetration effects

The upstream separatrix density is to a large extent determined by power flow, parallel conductivity, sheath physics and particle throughput. The physics is treated by code packages like B2-EIRENE and maximum values for ITER are expected to be around $n_{e,sep} = 3.5 10^{19}$ m^{-3} [10]. The key question for a device like ITER is which pedestal density can be achieved under given SOL and divertor conditions. An important topic in this context is the relative importance of neutral penetration versus transport physics. Fig. 2 shows the electron temperature and density widths and a regression for the

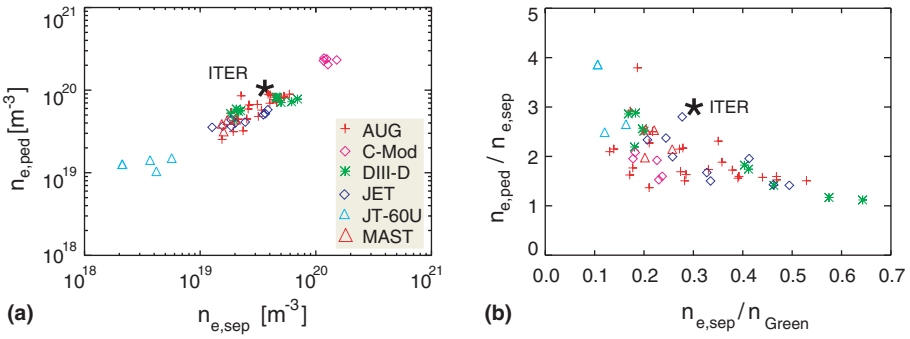

Fig. 1. (a) Pedestal density versus separatrix density and (b) $n_{e,ped}/n_{e,sep}$ versus $n_{e,sep}$ normalised by the Greenwald density. The data base comprises 28 type-I ELMy H-mode phases from AUG, 10 from DIII-D, 9 from JET, 4 from JT-60U, 1 ELMy and 4 EDA H-modes from C-Mod and 4 ELMy discharges with mixed type-I, III characteristics from MAST high-field side measurements. The ITER operating point assumes a pedestal density of 10.5 and a separatrix density of $3.5 \times 10^{19} m^{-3}$ [10].

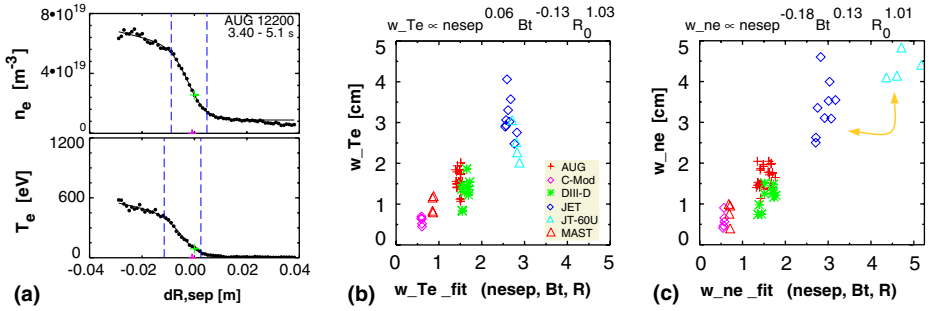

Fig. 2. Full widths of the temperature (b) and density (c) steep gradient zones taken from the tanh fit analysis versus 3-parameter fits for the dependence on separatrix density, toroidal field and major radius. As example for the determination of the full widths, edge profiles of n_e and T_e from ASDEX Upgrade are shown in (a). The barrier top and bottom positions obtained from the modified tanh fit are marked by vertical dashed lines. A full description of the tanh fit and its coefficients is given in [2].

dependence on $n_{e,sep}$, B_t and major radius R_0. Obviously, the leading parameter is the machine size, but a difference is seen in the density dependence of temperature and density widths. The uncertainty of the regression coefficients is about 0.3, the weak B_t dependence was also checked by omitting the C-Mod data (highest B_t in the database), which resulted in changes of the coefficients by less than 0.1.

The density pedestal profile in DIII-D has been described with an analytical model based on neutral penetration physics [11]. Since this model predicts tanh-function like density profile shapes, it can be easily compared with the present multi-machine data. With a slightly simplified version of the model, the density pedestal top position is taken to be the analytical neutral penetration depth, $w_{n,ana}$:

$$w_{n,ana} = \frac{2v_n f^{2ndCX}}{S_i n_{e,ped} E^*}, \quad v_n = \left(\frac{2eT_{i,sep}}{\pi M_i}\right)^{0.5}. \tag{2}$$

The neutral velocity v_n is assumed to be caused by a charge exchange process around the separatrix assuming $T_{i,sep} = 2T_{e,sep}$ [eV], $f^{2ndCX} = 2S_i/(S_i + S_{CX})$ is a correction factor taking a second charge exchange process into account. $S_{i,CX}$ are the rate coefficients for ionisation and CX, respectively. E^* is the neutral density weighted flux expansion wrt. the outer midplane. We use here the value $E^* = 7$ as suggested in [11], assuming dominant fueling at the X-point region with its large flux expansion. In contrast, dominant omp. fueling would mean $E^* = 1$. Fig. 3(a) compares the prediction of the analytical model with the measured density width inside the separatrix. There is considerable scattering, but one has to bear in mind that there is no free fitting parameter at all in the analytical model. Fig. 3(b) shows the width of the density barrier part situated inside the separatrix divided by the full barrier width. The reduction of this ratio with increasing Greenwald fraction of the separatrix density indicates an outward shift of the density profile. This tends to the direct effect of neutral penetration on one side (outward shift of the density profile with rising $n_{e,sep}$) and to the influence of transport (variation of edge transport with plasma current entering by n_{Green}) on the other side.

The most uncertain quantity in the analytical model is E^*, which takes into account the fueling location.

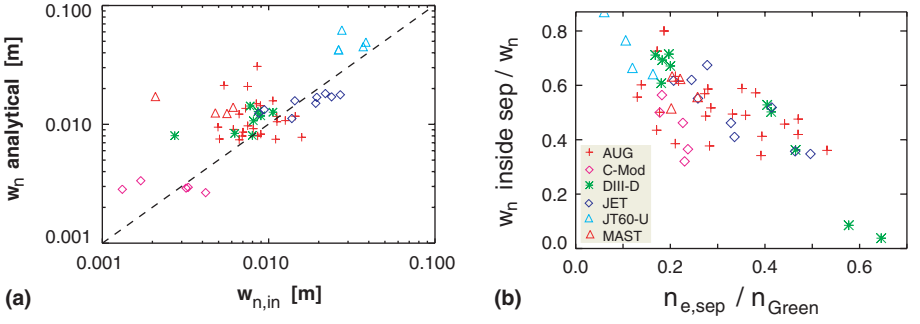

Fig. 3. (a) Measured density width versus neutral penetration depth from the analytical model. (b) Width of the density barrier part situated inside the separatrix divided by the full barrier width as obtained from the tanh analysis versus normalised separatrix density. The width ratio indicates the relative position of the density profile barrier region wrt the separatrix.

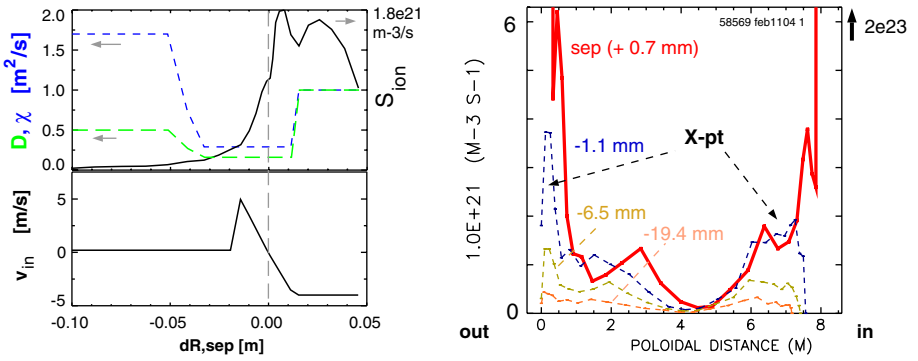

Fig. 4. Radial (outer midplane) and poloidal profiles of the neutral ionisation rate from EDGE2D calculations of a JET ELMy H-mode discharge. The transport coefficients are also shown to indicate the ETB position. The poloidal distribution shown on the rhs shows a high neutral source rate around the X-point outside the separatrix, which decays very fast towards the core.

Since the poloidal fueling distribution is normally not resolved by measurements due to lacking radial resolution, modelling has to be used to interpolate various experimental data. Fig. 4 shows neutral ionisation profiles for a JET ELMy H-mode discharge [7]. The neutral penetration depth is of the order of the density pedestal width, but an inward drift had to be employed to model the inner part of the steep density gradient zone. The (arbitrary) combination of a diffusion coefficient and inward drift reflects the importance of transport processes for the density profile shape. The poloidal neutral distribution shows a high source rate at the separatrix up to the X-point region. However, the neutrals are well ionised over the large flux expansion around the X-point and only a weak poloidal variation of the source rate remains inside $R - R_{sep} = -1$ cm (mapped to outer midplane). Consequently, the JET modelling results suggest a smaller value of E^* compared to DIII-D, namely $E^* \approx 2$–3. In summary of the edge density profile analysis, a more comprehensive multi-machine analysis is required, using 2-d kinetic calculations closely connected to experimental data with high spatial resolution.

2.2. Temperature and power decay length

The most important parameter for target power handling in ITER is the power decay length. The electron temperature profiles compiled in this database give radial e-folding lengths of T_e, Fig. 5 shows λ_{T_e} values derived from the profile fits at the separatrix in the outer midplane. The temperature decay lengths translate into midplane power e-folding lengths $\lambda_{q\perp} = 2/7\ \lambda_{T_e}$ for cases with dominant electron thermal conduction, namely not too low ion collisionality [9]. When testing against various regression quantities, like major radius, heating power, safety factor or separatrix density, linear dependence of λ_{T_e} on R_0 is found, while all other quantities show a power law dependence with non-significant exponents less than 0.2. Fig. 5(b) shows the dependence of λ_{T_e}/R_0 on the normalised separatrix density. The major radius as size parameter gives less scatter than the minor radius, revealing unresolved effects of geometrical moments like δ, κ [12]. R_0 is used here because a better fit is obtained. MAST data are not included since the Thomson scattering does not allow to directly determine λ_{T_e} at the separatrix. The probe measurements

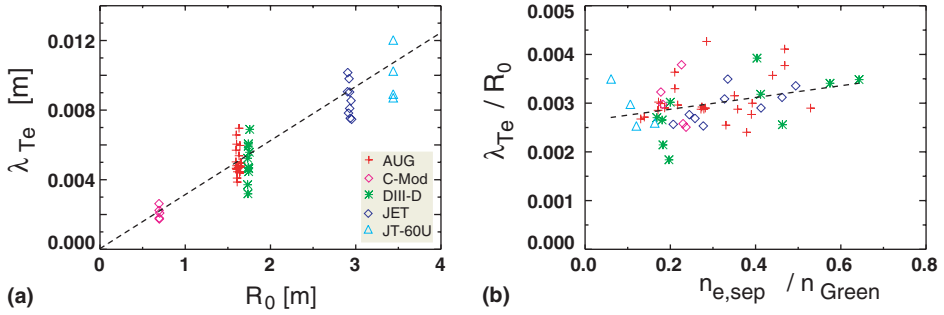

Fig. 5. (a) Midplane temperature e-folding length versus major machine radius R_0. The dashed line shows $\lambda_{T_e} = 3.1 \times 10^{-3} R_0$ obtained from fitting. (b) λ_{T_e} normalised by machine size versus normalised separatrix density.

mentioned above indicate much higher values of λ_{T_e}/R_0 compared to the high aspect ratio tokamaks, suggesting that in fact the minor radius is the more appropriate size parameter.

The normalised density gradient lengths at the separatrix exhibit a higher scatter when plotted according to Fig. 5(b), but its average value is 2 times the value for λ_{T_e}/R_0. This is compatible with $\eta_e = \lambda_{n_e}/\lambda_{T_e} \approx 2$ as observed in ASDEX Upgrade over the whole edge transport barrier region [13].

3. Conclusions and outlook

The multi-machine database for H-mode edge profiles set up under the framework of the ITPA Divertor and SOL Topical Group has unveiled effects related to transport as well as neutral penetration physics to effect the buildup of the edge/pedestal density profile. The implications of neutral physics are related to the ionisation length, however, the poloidal source distribution is important due to the strongly varying flux expansion. Transport effects can be related to effects of intermittent transport in the outer SOL and to the coupling of electron temperature and density gradient length over the edge transport barrier region as observed in ASDEX Upgrade [13]. The leading parameter for the edge widths and decay lengths considered is the machine size, which is related, e.g., to the width of the region with strong magnetic shear.

Without the physics of the edge transport barrier fully understood, a prediction for the edge density profile in ITER is uncertain. The diagram of $n_{e,ped}/n_{e,sep}$ versus the Greenwald fraction of the separatrix density as shown in Fig. 1(b) appears to be the best empirical normalisation. In this diagram, the aspired density rise factor $n_{e,ped}/n_{e,sep}$ for ITER is slightly higher compared to typical values achieved with gas fueling in present day experiments. The relation $\lambda_{T_e} = 0.003 \cdot R_0$ would result in a midplane electron temperature decay length in ITER of about 2 cm. More detailed modelling will be required to improve the ITER predictions and to investigate, e.g., the effect of edge fueling with pellets. As a consequence, a combined effort has been launched recently by the ITPA Pedestal and Divertor&SOL Topical Groups to combine multi-code, multi-machine modelling with a new international pedestal database based on standardised MDS + interfaces.

Acknowledgments

This work was supported in part by US Department of Energy under DE-FC02-04ER54698 and W-7405-ENG-48.

References

[1] D. Mossessian et al., Plasma Phys. Control. Fus. 42 (2000) A255.
[2] A. Kallenbach et al., Nucl. Fus. 43 (2003) 573.
[3] G. Porter et al., Phys. Plasmas 5 (1998) 1410.
[4] A. Kirk et al., Plasma Phys. Control. Fus. 46 (2004) 551.
[5] M. Kempenaars et al., in: 30th EPS Conf. on Contr. Fusion and Plasma Phys., St. Petersburg, vol. 27A, ECA, 2003, EPS, 2003.
[6] Y. Kamada et al., Plasma Phys. Control. Fus. 41 (1999) 1371.
[7] A. Kallenbach et al., Plasma Phys. Control. Fus. 46 (2004) 431.
[8] N. Asakura et al., Nucl. Fus. 39 (1999) 1983.
[9] W. Fundamenski et al., Nucl. Fus. 44 (2004) 20.
[10] A. Kukushkin, H. Pacher, Plasma Phys. Control. Fus. 44 (2002) 931.
[11] M. Mahdavi et al., Phys. Plasmas 10 (2003) 3984.
[12] M. Sugihara et al., Plasma Phys. Control. Fus. 45 (2003) L55.
[13] J. Neuhauser et al., Plasma Phys. Control. Fus. 44 (2002) 855.